

Prediction of the Charge Transport and Electronic Properties of Two Pyrazole Derivatives in terms of Their Solid Molecular Arrangements and Reorganization Energy: The Effects of Nitro Groups on Structure-Property Relationship

Abdullah Biçer¹, Günseli Cin², and Gül Yakalı³

¹Gebze Technical University

²Akdeniz Universitesi

³Izmir Katip Celebi Universitesi

September 27, 2022

Abstract

Pyrazole derivatives have noteworthy attention in optoelectronic field since they demonstrate distinctive properties in semiconducting devices such as organic light emitting diodes (OLEDs), nonlinear optical (NLO) and solar cells. organic field effect transistors (OFETs). Therefore, to establish the relationship between the structure and property of the molecules, we explored influence of nitro groups on the 3D molecular structures, reorganization energy, absorption spectra, frontier orbitals, ionization potential (IP), electronic affinity (EA), intra-molecular charge transfer (ICT) and charge transport behaviour of the two π -conjugated pyrazole compounds through single crystal x-ray crystallographic and quantum chemical calculations by considering Marcus Electron Transfer Theory and Density Functional Theory. Our experimental and theoretical results predicted that incorporation of the nitro groups to the molecule skeleton increased the rigidity of the conjugated system and improve the efficient charge injection in electronic devices by lowering the hole (λ_h) and electron (λ_e) reorganization energy from 0.48eV to 0.34 eV, 0.44 eV to 0.26 eV, respectively which can be effective way to design molecules with desired electronic properties via smart chemical structural modification. In addition, both molecules aggregate with the close preferred π [?]p stacking interactions (J and antiparallel H type) and multiple intermolecular interactions in their solid phases. Accordingly, both molecules are suggested to be quite suitable for p-type semiconducting materials with small reorganization energy and preferred stacking modes in solid phase. In addition, this study paves the way for the design and synthesis of new conjugated pyrazole molecules for high device performance.

Introduction

Organic semiconductors are best candidate materials for organic field-effect transistors (OFETs), organic light-emitting diodes (OLEDs), and organic photovoltaic cells (OPVCs) since they have enormous properties such as mechanical flexibility, light weight, bulk chemical synthesis and low-cost organic electronic devices [1–4]. Ability to adjust the properties of the organic semiconductors including mostly π -conjugated molecules through the chemical tailoring of the molecular structure is their most important advantage for application of the optoelectronic devices[5–8]. To create semiconducting materials with various properties in organic electronic devices, subtle modification such as incorporation various heterotams to organic compounds can be performed. Therefore, understanding the structure-property relationship which is one of the most fundamental researchwork in organic semiconductors today has vital role in the optic-electronic field that it is becoming increasingly needed area in order to improve the properties of the functional materials in the best way for their applications [9, 10]. For this purpose, single crystal x-ray diffraction (SCXRD) is

the most strongest method for analysing the structure-property relationship of the π -conjugated molecules in terms of their molecular arrangements in aggregation phase and charge transport properties[11–13]. A detailed analysis on the between solid-state molecular arrangements (molecular packing) and charge transport characteristics in molecular crystals bring a solution if and how the materials might eventually be used in device fabrication, and how the transporting properties of materials can be designed in order to improve their electronic applications.

The organic single crystal structure of the π -conjugated molecules can provide detailed information on the 3D molecular structure, molecular arrangements, and noncovalent interactions including intermolecular and intramolecular nonclassical hydrogen bonds, $C-H \cdots \pi$, $X-Y \cdots \pi$, $\pi \cdots \pi$ stacking and strong short interactions in aggregate phase [12, 14–18]. The determination of these features gives excellent information about the functional material properties which are performed by the whole collective of organic fragments not only of single molecules themselves and these collective arrangements offer intrinsic properties with different molecular packing created by noncovalent interactions [18–22]. Therefore, to perform the optimized optical and electronic properties in molecular and supramolecular levels, manipulation of the molecular packing and intermolecular interactions are arguably a main issue since molecular arrangements between the neighboring molecules in solid phase has considerably effect on charge transport properties of the molecules [23–26]. They can form different solid state packing geometry in different directions which results in different transport properties and anisotropies.

$\pi \cdots \pi$ stacking interactions including types edge-to-face T-shape, parallel or antiparallel displaced (J type), and cofacial parallel or antiparallel stacked (H type) are one of the most important noncovalent interactions between the molecular orbitals in supramolecular level to elucidate the charge transport feature based on the aggregation phase of the neighboring molecules[27–31]. The principle account of the stacking interactions is that the electron-withdrawing substituents tend to enhance the $\pi \cdots \pi$ stacking interaction while electron-donating substituents reduce. Thus, co-facial $\pi \cdots \pi$ stacking is generally not preferred for aromatic compounds because of quadrupole repulsion. In terms of the electronic model of the molecules, $\pi \cdots \pi$ interactions between the HOMO and LUMO orbitals which created antiparallel stacking modes J or H type more beneficial for the efficient charge transport than HOMO-HOMO or LUMO-LUMO orbital overlaps. Due to the fact that charge pathways between the adjacent rings in solid phase created by the $\pi \cdots \pi$ stacking interactions, specifying the perpendicular distance (d) between the rings, pitch and roll distances and angles are important issue to determine whether the interactions are strong and their stacking types. The stronger interaction formed by the small d value with the favourable stacking type (antiparallel H and J) results in more efficient charge transport in solid phase[32–34].

Beside the molecular packing of the molecules, the charge transfer rate which relates to the parameters of reorganization energy and charge transfer integral is important parameter to set up the structure-property relationship in optoelectronic device performance[35–38]. Charge transfer integral is related to intensity of electronic coupling constant which associated with geometry of the stacking interactions including perpendicular distance between the rings, pitch and roll distances and angles, and stacking type of the molecules in solid phase[39–42]. According to experimental and theoretical studies more overlap between the adjacent rings with the favourable stacking type result in high electronic coupling therefore high charge transfer integral which is desired to be high for efficient charge transfer rate verified by Marcus Electron Theory[43]. Therefore, along with examining the single crystal structure and electronic interactions of the molecules, it is necessary to carry out the theoretical investigations to predict the charge transport rate of the practical materials. The reorganization energy determine the change in energy of the molecule because of the presence of excess charge and the surrounding medium [44]. Minimization of reorganization energy and maximization of transfer integral are considered suitable for molecular design.

In this study, to fully understanding the structure-property relationships and to predict the charge carrier mobility in terms of microscopic point of view, the effects of the molecular packing, noncovalent interactions and the crystal geometry on the charge transport properties by considering the reorganization energy of the molecules were investigated through crystallographic and theoretical studies of the typical two pyrazole

derivatives. The molecules have electron-rich pyrazole moiety which attains conjugation by donating electron, so it behaves as a donor-acceptor type of functional molecules. Therefore, pyrazole derivatives generally have been used as hole transport materials. In the same way we have found that, both molecules show hole transport properties due to effect of the heteroatom brom and electron withdrawing nitro groups. The 3D molecular structures, reorganization energy, electronic properties including absorption spectra, frontier orbitals, ionization potential (IP) and electronic affinity (EA), crystal packing modes of both compounds were calculated to analyze the relationship between structures and properties and therefore to lead the way on designing new pyrazole derivative organic semiconductors with good charge transport rate.

Experimental Studies

All chemicals were obtained from Sigma-Aldrich, and were used without further purification. ^1H NMR and ^{13}C NMR spectra were recorded on a Varian 200 MHz or Bruker Avance DPX 400 MHz spectrometer using CDCl_3 as a solvent and tetramethylsilane (TMS) as an internal standard. Splitting patterns are designated as follows; s, singlet; d, doublet; m, multiplet. Chemical shift (δ) values are given in ppm.

Synthesis

AB1 and **AB2** molecules were synthesized using the reaction pathway in Scheme 1[45–48]. First of all, pyrazole derivatives were synthesized from acetylacetone (**1**). Then, bromination reactions were carried out in a regioselective manner using different bromination conditions.

Scheme 1. The reaction pathway for **AB1** and **AB2** molecules

General procedure for synthesis 3,5-dimethyl-1-aryl-1H-pyrazole derivatives (3a-b)

To a solution of acetylacetone (98 mmol) in ethanol (150 mL), aryl hydrazine (97.37 mmol) was slowly added. After cooling the reaction mixture to 0°C , 5 mL of concentrated hydrochloric acid was added. The reaction mixture was refluxed for 2 hours. After the reaction was complete, ethanol was evaporated, then the crude product was dissolved in DCM. The reaction mixture was treated with 10 % NaOH solution to slightly basic (pH around 9). After this mixture was extracted with dichloromethane (2x100 mL), the combined dichloromethane solution was washed with brine and dried over anhydrous sodium sulfate. The product was purified using column (EtOAc:hexane; 2:8)

3,5-dimethyl-1-phenyl-1H-pyrazole (3a): Yield 94%; red liquid; ^1H NMR (400 MHz, CDCl_3) δ 7.38-7.23 (m, 5H), 5.94 (s, 1H), 2.25 (s, 3H), 2.24 (s, 3H). ^{13}C NMR (101 MHz, CDCl_3) δ 148.92, 139.96, 139.34, 128.97, 127.20, 124.72, 106.93, 13.51, 12.36.

1-(2,4-dinitrophenyl)-3,5-dimethyl-1H-pyrazole (3b): Yield 90%; yellow solid; ^1H NMR (400 MHz, CDCl_3) δ : 8.80 (d, $J = 4.0$ Hz, 1H), 8.55 (dd, $J = 8.0$ Hz, 4.0 Hz, 1H), 7.72 (d, $J = 8.0$ Hz, 1H), 6.12 (s, 1H), 2.29 (s, 3H), 2.27 (s, 3H). ^{13}C NMR (101 MHz, CDCl_3) δ 152.36, 146.22, 145.64, 140.90, 137.95, 129.33, 127.34, 120.99, 108.90, 77.38, 77.06, 76.74, 13.48, 11.61.

General procedure for synthesis 4-bromo-3,5-dimethyl-1-aryl-1H-pyrazole derivatives (4a-b):

A mixture of 3,5-dimethyl-1-aryl-1H-pyrazole (23 mmol) and NBS (132 mmol) in acetone (100 mL) was irradiated under an ultrasonic wave in a $25\text{--}30^\circ\text{C}$ bath for 2 h. The solution was concentrated and reaction mixture was extracted with EtOAc. After the resulting residue was purified using column (EtOAc:hexane; 2:8)

4-bromo-3,5-dimethyl-1-phenyl-1H-pyrazole (4a): Yield 75%, brown solid, ^1H NMR (400 MHz, CDCl_3) δ 7.40-7.29 (m, 5H), 2.28 (s, 3H), 2.25 (s, 3H). ^{13}C NMR (101 MHz, CDCl_3) δ 147.47, 139.76, 137.43, 129.13, 127.75, 124.58, 96.43, 12.35, 11.74.

4-bromo-1-(2,4-dinitrophenyl)-3,5-dimethyl-1H-pyrazole (4b): Yield 70%, bright yellow solid ^1H NMR (400 MHz, CDCl_3) δ 8.85 (d, $J = 4\text{Hz}$, 1H), 8.58 (dd, $J = 8.0$, 4.0 Hz, 1H), 7.71 (d, $J = 8.0$ Hz, 1H), 2.29 (s, 6H). ^{13}C NMR (101 MHz, CDCl_3) δ 152.78, 144.94, 138.31, 130.18, 129.56, 123.45, 116.31, 77.33, 77.22, 77.01, 76.70, 48.27, 16.01.

General procedure for synthesis 4-bromo-5-(bromomethyl)-3-methyl-1-aryl-1H-pyrazole (AB1, AB2):

A mixture of 4-bromo-3,5-dimethyl-1-aryl-1H-pyrazole (11.5 mmol) and NBS (66 mmol) in benzene (50 mL) was refluxed for 4 day. The solution was concentrated, reaction mixture was extracted with EtOAc. After the resulting residue was purified using column (EtOAc:hexane; 1:9)

4-bromo-5-(bromomethyl)-3-methyl-1-(p-tolyl)-1H-pyrazole (**AB1**): Yield 45%, white solid, ¹H NMR (400 MHz, CDCl₃) δ 7.48 (d, *J* = 8.0 Hz, 2H), 7.42 (t, *J* = 8.0 Hz, 2H), 7.34 (t, *J* = 8.0 Hz, 1H), 4.33 (s, 2H), 2.23 (s, 3H). ¹³C NMR (101 MHz, CDCl₃) δ 148.32, 139.02, 136.87, 129.46, 128.66, 124.70, 98.52, 77.42, 77.10, 76.78, 20.20, 12.26.

4-bromo-5-(bromomethyl)-1-(2,4-dinitrophenyl)-3-methyl-1H-pyrazole(**AB2**): Yield 55%, green solid, ¹H NMR (400 MHz, CDCl₃) δ 8.86 (t, *J* = 2.0 Hz, 1H), 8.65 (dt, *J* = 8.0, *J* = 2.0 Hz, 1H), 8.04 (dd, *J* = 8.0, *J* = 2.0 Hz, 1H), 4.43 (s, 2H), 2.29 (s, 3H). ¹³C NMR (101 MHz, CDCl₃) δ 151.41, 147.33, 146.05, 138.32, 136.71, 129.31, 127.76, 121.28, 100.64, 18.59, 12.31.

Crystallograpy

By using the Rigaku Oxford XCalibur diffractometer including EOS CCD detector with MoK_α radiation ($\lambda = 0.7107$) at room temperature, the single crystallographic datas of two pyrazole derivatives were obtained. CrysAlis^{Pro} software package was utilised to perform data collections, cell refinements, data reductions and absorption corrections [49]. Structure solution and refinement process for both compounds were analysed by considering direct methods with SHELXT and SHELXL respectively in OLEX2 software [50–52]. All atoms except the hydrogen atoms were taken into account as an anisotropic thermal ellipsoids. The riding model was used to determine the positions of hydrogen atoms. Crystallographic data of both molecules are offered in Table 1.

Table 1 . Crystallographic details for the molecules.

Name	AB1	AB2
Empirical formula	C ₁₁ H ₁₀ Br ₂ N ₂	C ₁₁ H ₈ Br ₂ N ₄ O ₄
Formula weight	330.03	420.02
Temperature (K)	297(2)	296(2)
Crystal system	monoclinic	triclinic
Space group	C2/c	P-1
<i>Unit cell dimensions a</i> (Å) <i>b</i>	16.0133(18) 7.4213(12)	8.4425(7) 9.9723(8) 10.2733(14)
(Å) <i>c</i> (Å) α (°) β (°)	19.871(3) 90 93.484(12) 90	64.960(10) 66.421(10) 82.487(7)
γ (°)		
Volume/(Å ³)	2357.1(6)	717.43(15)
<i>Z</i>	8	2
<i>D</i> _{calc} (g/cm ⁻³)	1.860	1.9442
Absorption coefficient (mm ⁻¹)	6.846	5.670
<i>F</i> (000)	1280.0	407.1
Crystal size (mm)	0.267 × 0.121 × 0.059	0.357 × 0.211 × 0.129
<i>h</i> ranges	-13-18	-10-9
<i>k</i> range	-8-8	-12-12
<i>l</i> range	-23-21	-10-12
Reflections collected/unique	3705/2079	4241/2700
Data / restraints / parameters	2079/0/137	2700/0/191
Goodness of fit on <i>F</i> ²	0.962	1.061
Final <i>R</i> indices [<i>I</i> > 2σ(<i>I</i>)]	R ₁ = 0.0576 wR ₂ = 0.1058	R ₁ = 0.0496 wR ₂ = 0.0774
<i>R</i> indices (all data)	R ₁ = 0.1459 wR ₂ = 0.1375	R ₁ = 0.0931 wR ₂ = 0.0938

Largest difference peak and hole 0.47/-0.50 0.74/-0.85
 (e Å⁻³)

Theoretical Methodology

The optimized geometries of the neutral and charged states of the molecules were generated at the DFT level using B3LYP hybrid functional and 6-31 G**(d,p) basis set which are considered to provide enough accuracy as performed in the Gaussian 09 package [53]. The electronic excitation energies and the absorption spectra for two pyrazole derivatives in the absence of solvent are computed with the time-dependent density functional theory (TD-DFT) at the B3LYP/6-31G** (d,p) level. In addition, the molecular ionization potential (IP) and electron affinity (EA), inner reorganization energy were calculated [54].

Result and Discussion

Molecular Structure Description

When the functional groups bound to the terminal region of the molecules, this situation results in significant discrepancy in the 3D molecular structure and molecular packaging. The types of crystal packagings are determined by single crystal analysis and this discrepancy is very important in the determining charge transport properties of the molecules in the optoelectronic field. Therefore, the single x-ray diffraction analysis (SCXRD) was performed to analyze charge transport properties of **AB1** and **AB2** molecules by utilising their 3D molecular structures and packing arrangements in solid phase. Thermal ellipsoid views of the both molecules are presented in Figure 1. Table 2 shows selected bond lengths and angles of the molecules which are very compatible similar studies in the literature[54–56]. Beside, geometrical parameters of both compounds compared with the results obtained from theoretical calculations. SCXRD bring to light that **AB1** and **AB2** crystallize in the monoclinic space group C2/c and triclinic space group P-1, respectively.

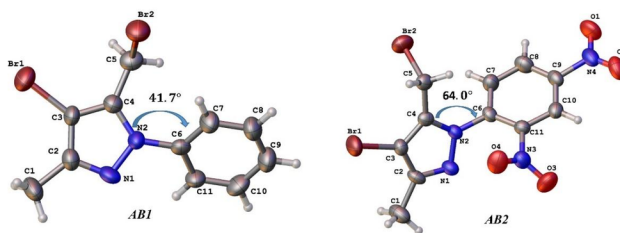


Figure 1. The thermal ellipsoids views of the molecules with 50% possibility.

Table 2. Selected geometrical parameters of the molecules.

Bond Lengths (Å) Experimental	Bond Lengths (Å) Experimental	Bond Lengths (Å) Calculated	Bond Lengths (Å) Experimental	Bond Lengths (Å) Experimental	Bond Lengths (Å) Calculated
AB1	AB1	AB1	AB2	AB2	AB2
Br1–C3	1.876(8)	1.88(2)	Br1–C3	1.868(5)	1.8682(8)
N2–C4	1.351(10)	1.37(2)	N2–C4	1.351(6)	1.3500(10)

Br2–C5	1.980(8)	2.01(2)	Br2–C5	1.954(5)	1.9543(2)
N2–C6	1.419(10)	1.42(2)	N2–C6	1.524(7)	1.425(2)
N1–N2	1.374(9)	1.354(2)	N1–N2	1.368(6)	1.368(2)
N1–C2	1.321(12)	1.32(2)	N1–C2	1.334(8)	1.333(2)
			N3–C11	1.477(7)	1.476(2)
			N4–C9	1.479(8)	1.478(2)
			N4–O1	1.223(7)	1.223(2)
			N3–O3	1.216(7)	1.216(2)
Bond Angles()					
AB1	AB1	AB1	AB2	AB2	AB2
N2–N1–C2	106.1(7)	106.6(2)	N2–N1–C2	104.0(4)	103.99(2)
N1–N2–C4	109.8(6)	111.8(2)	N1–N2–C4	113.1(4)	113.1(2)
N1–N2–C6	118.7(6)	118.5(2)	N1–N2–C6	118.4(4)	118.39(2)
Br1–C3–C2	126.4(6)	126.8(2)	Br1–C3–C2	127.4(4)	127.4(2)
Br1–C3–C4	126.2(9)	126.2(2)	Br1–C3–C4	124.7(4)	124.7(2)
Br2–C5–C4	111.5(5)	113.5(2)	Br2–C5–C4	112.3(3)	112.3(2)
N2–C6–C7	120.2(7)	120.9(2)	N2–C6–C7	119.4(5)	119.31(2)
C4–N2–C6	129.5(9)	129.4(2)	C4–N2–C6	128.3(4)	128.27(2)
C1–C2–C3	131.5(6)	129.02(2)	C1–C2–C3	128.4(6)	128.38(2)
N2–C6–C11	119.9(7)	118.5(2)	N2–C6–C11	121.8(5)	121.78(2)
			N3–C11–C10	117.1(5)	117.1(2)
			N4–C9–C10	118.1(5)	118.1(2)
			O1–N4–O2	125.0(6)	124.98(2)
			O3–N4–O4	124.5(5)	124.49(2)

It can be seen that the phenyl groups in molecules are conjugated with the pyrazoline ring and create conjugated π system. The dihedral angles between phenyl and pyrazole rings of the **AB1** and **AB2** connected with the N–C bonds [N–C: 1.419 for **AB1** 1.420 for **AB2**] are 41.7 and 64.0, respectively. The discrepancy between the dihedral angles are attributed to the introduction of the sterically hindered nitro (NO₂) groups which decreases the planarity of the molecular structure in solid phase. The internal rotations of the **AB1** are restricted by strong short interactions [Br2 \cdots H7: 2.96 Å] while that of **AB2** are provided by intramolecular N–O \cdots π interactions (Table 3). Pyrazole and phenyl rings of the **AB1** make the angle of 16.8(4) and 24.9(3) with the molecule plane, respectively whereas for **AB2**, these angles are 40.6(2) and 23.34(2) Since there are no nonclassical hydrogen bonds and X–Y \cdots ring interactions in the crystal structure of compound **AB1**, the only strong intermolecular $\pi\cdots\pi$ stacking interactions and short interactions are responsible for its rigid structure in aggregation or packing phase. However, the molecule **AB2** has intermolecular nonclassical hydrogen bonds, X–Y \cdots ring interactions and strong $\pi\cdots\pi$ stacking interactions in solid phase due to the presence of the electron withdrawing groups (NO₂) connected to phenyl ring in its terminal side (Table 3).

Table 3. Molecular noncovalent interactions geometry of the molecules (Å, °).

Nonclassical Hydrogen Bonds	Nonclassical Hydrogen Bonds	Nonclassical Hydrogen Bonds	Nonclassical Hydrogen Bonds
Molecule	D–H[?][?][?]A	D–H	H[?][?][?]A
AB2	C1–H1B[?][?][?]O1	0.96(3)	2.59(3)
	C5–H5A[?][?][?]O2	0.971(7)	2.562(7)
Y–X$\cdots$$\pi$ Interactions	Y–X$\cdots$$\pi$ Interactions	Y–X$\cdots$$\pi$ Interactions	Y–X$\cdots$$\pi$ In
AB2	Y–X[?][?][?]Cg	X[?][?][?]Cg	Y–X[?][?][?]
	C5–Br1[?][?][?]Cg1	3.529(2)	140.31(16)
	N4–O1[?][?][?]Cg2	3.653(5)	71.0(3)
	N4–O2[?][?][?]Cg2	3.317(5)	86.1(3)

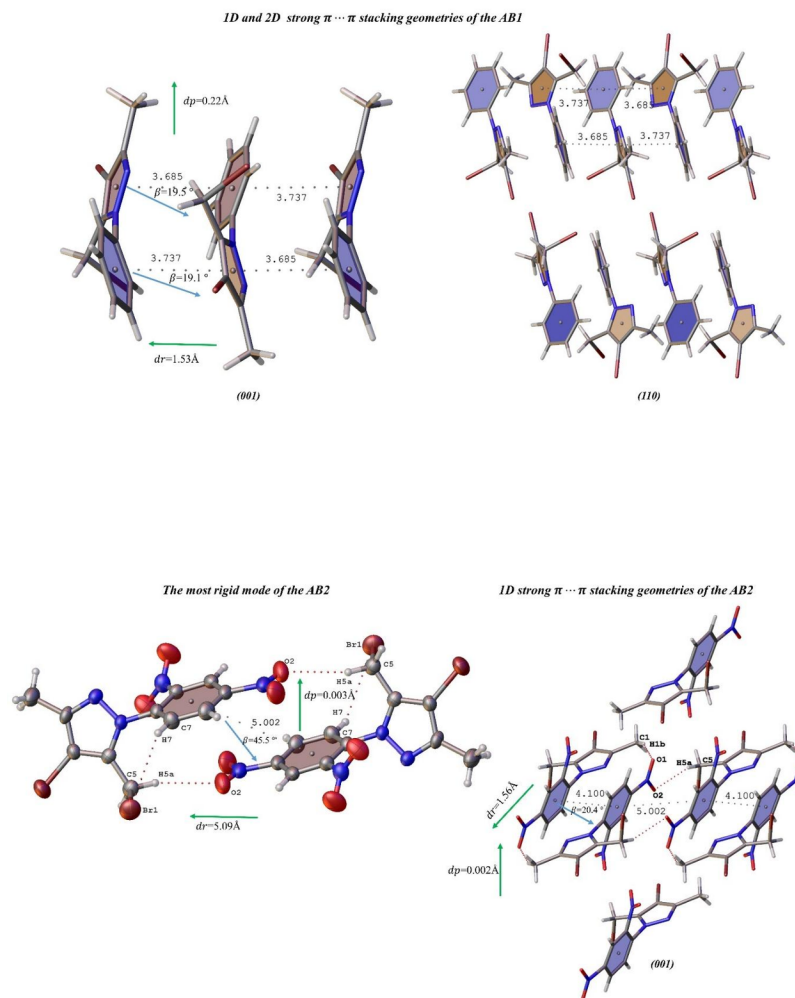


Figure 2. Aggregation modes of the both molecules in their solid phases with the noncovalent interactions.

The molecule **AB1** demonstrates stacking columns along the c-axis where the molecules adopt a slipped antiparallel face-to-face (H type) packing style [Cg2Cg1; Cg1: N1-N2-C2/C4, Cg2:C6/C11, symmetry code: $1/2-x, -1/2+y, 1/2-z$ for 3.68, $1/2-x, 1/2+y, 1/2-z$ for 3.74] which have shifting along the long and short molecular axis (roll distance (dr): 1.53; pitch distance (dp): 0.22) and an interplanar distance of 3.68 and 3.74 with the slipping angle of 19.5° (Figure 2). The molecule **AB2** packs in antiparallel displaced stacking modes (J type) [Cg2Cg2; Cg2:C6/C11, symmetry code: $2-x, 1-y, 1-z$] in its crystals structure and the molecule is replaced mostly along the long molecular axis with an interplanar distance of 5.002 (Figure 2) with the slipping angle of 45.5°. When the interplanar distance is 4.10 between the adjacent rings of the **AB2** [Cg2Cg2; Cg2:C6/C11, symmetry code: $1-x, 1-y, 1-z$], its aggregation mode behaves nearly antiparallel H type stacking mode with the small slipping angle of 20.4°. These two stacking modes of the **AB2** demonstrate the charge pathways in its solid phase. Therefore, the attaching of these substitution groups leads to striking changes in molecular aggregation. Small perpendicular distance with the J type and antiparallel H type

stacking modes is desired property for the high charge transfer rate[2, 57, 58]. In addition, the rigidity of the molecules in solid state increases the charge transport which arise from restricted intra-intermolecular rotation process (RIR). The RIR process is created by the noncovalent interaction observed in the both molecules. According to SCXRD results, It is predicted that this series of pyrazole derivatives can be good candidate for ambipolar semiconducting materials when they are used as a device in real world since they have favourable strong stacking modes (J and H type)

Interpretation of charge transport properties

Predicting the charge transfer rate of the molecules

The intramolecular charge transfer properties (ICT) of the two pyrazole derivatives were interpreted by considering molecular frontier orbitals energy levels and energy band gap ($E_{\text{band gap}}$). The optimized structures in the neutral state of AB1 and AB2 which are quite compatible with 3D molecular view are presented in the Figure 3.

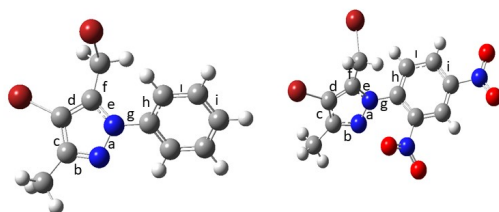


Figure 3. Neutral optimized structures of the AB1 and AB2.

The torsional angles between the phenyl and pyrazole rings of AB1 and AB2 are 46.12° and 56.99° in gas phase which is in good agreement with that of solid phases of the molecules (41.7° and 64.7° for **AB1** and **AB2**). When a molecule gains or loses charges, it will relax its molecular geometry for a new charge distribution[44, 59, 60]. Therefore, torsional angles in **AB1** are 36.03° and 22.33° for the anionic state and cationic state, respectively while **AB2** has torsional angles of 56.82° and 66.97° for the anionic state and cationic state, respectively. The change of torsion angles in the cationic state for both molecules is more dominant than those in the anionic state compared with the neutral state, specifying that the hole reorganization energy is smaller than those of electron[61–63].

The bond length changes due to oxidation (electron lose from the neutral to the cation state) and reduction (electron gain from the neutral to the anion state) of **AB1** and **AB2** are given in Table 4. The geometrical changes in **AB2** are more conspicuous than those in **AB1**, which can be taken into account as the effect of introduction of nitro groups in the molecule. For the investigated molecules, the hole reorganization energies are smaller than those of electron since the bond-length changes upon reduction are significantly larger than those upon oxidation. In addition, the outcomes obtained from the calculation of the hole and electron reorganization energies of the molecules listed in Table 6 confirm this result. According to Marcus Electron Theory, low reorganization energy is a desired property for high charge transport rate. As a result, it can be said that both compounds have hole transport property rather than electron.

Table 4 . Bond Length Alternation Values of the molecule **AB1** and **AB2**

Index	Notr	Anion	Cation	$\Delta(C - N)$	$\Delta(A - N)$
a	1.35433	1.35923	1.40188	0.04755	0.0049
b	1.32879	1.33582	1.30156	0.02723	0.00703
c	1.41077	1.39443	1.45803	0.04726	0.01634
d	1.38546	1.42044	1.38551	0.00005	0.03498
e	1.37606	1.39967	1.37825	0.00219	0.002361
f	1.46978	1.38664	1.47947	0.00969	0.08314
g	1.42730	1.42450	1.39069	0.03661	0.0028
h	1.39509	1.39519	1.41637	0.02128	0.00001
i	1.39345	1.39340	1.37927	0.01418	0.00005
i	1.39199	1.39174	1.40481	0.01282	0.00025

Table 5 . Bond Length Alternation Values of the molecule **AB2**

Index	Notr	Anion	Cation	$\Delta(C - N)$	$\Delta(A - N)$
a	1.36854	1.35578	1.41450	0.04596	0.01276
b	1.33364	1.33242	1.30129	0.00235	0.00122
c	1.38839	1.40481	1.45301	0.06462	0.01642
d	1.36171	1.42044	1.43686	0.07515	0.05673
e	1.47303	1.36736	1.32350	0.14953	0.10567
f	1.35009	1.46207	1.47603	0.12594	0.11198
g	1.42440	1.42336	1.42969	0.00529	0.00104
h	1.37570	1.43870	1.39253	0.01683	0.063
i	1.38878	1.39868	1.39318	0.0044	0.0099
i	1.36518	1.38113	1.38548	0.0203	0.01595

Table 6. The value of parameters determining the charge transfer property of the molecules.

Molecule	(eV)	(eV)	IPa (eV)	IPv(eV)	Ea(eV)	Ev(eV)
AB1	0.44	0.48	7.86	8.09	1.56	1.48
AB2	0.26	0.34	8.53	8.80	2.13	0.34

The nitro groups in the π system reduce the reorganization energies for both hole and electron[64]. The reorganization energy for hole of **AB1** and **AB2** are 0.44 eV and 0.26 eV, respectively, The higher reorganization energy is confirmed by a larger geometrical relaxation with respect to the neutral geometry (Table 4 and Table 5). The calculated results show that the incorporation of the NO_2 groups result in different charge transport property because of discrepancy between the reorganization energies for both compounds.

Molecular Ionization Potential and Electron Affinity

The injection of the holes and electrons is given considerable attention to create optimized electronic devices in real world. The information about the organic device performance and its stability can be obtained from the parameters of ionization potential (IP) and electronic affinity (EA) that determine the charge injection through estimating the energy barrier for injection of hole and electron into molecule.

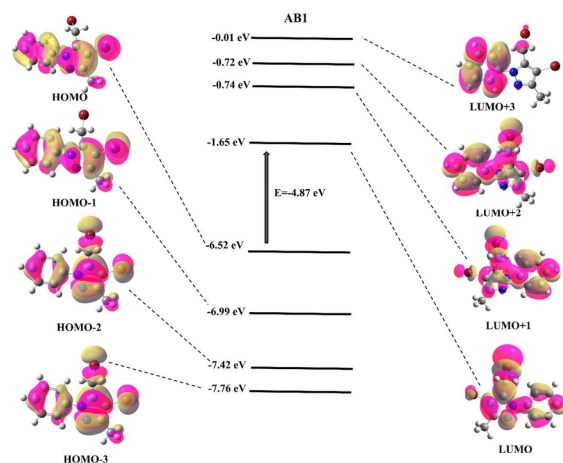
[65, 66]. The calculated IPs and EAs of compounds, both vertical (at the geometry of the neutral molecule) and adiabatic (optimized structure for both the neutral and charged molecules), are presented. More stable and hardly oxidized molecules are favoured for the practical applications that high IPs value provide these

features to the molecules [67]. When the Au is used as an electrode, **AB2** is predicted to has smaller injection energy for hole than **AB1**. The EA values of **AB1** and **AB2** are 1.56 and 2.13 eV, respectively (Table 6). For the devices if the EA value is high, it means that injection energy for electron will be small (commonly used metallic electrodes (3 eV)). From these EA values, we can see that **AB2** is better than **AB1** for transporting electrons from both lowering the energy barrier for electron injection.

Besides that, the HOMO energy levels for both compounds are good agreement with the work function of the gold electrode (-5.2 eV). Therefore, the injection of the hole from the gold to the organic semiconductor easily accomplished.

Frontier Molecular Orbitals

Frontier orbitals are parameters related to the state of a molecule gaining or losing electrons. In this study, the incorporation of nitro groups to the terminal sides of the **AB1** considerably affect the atomic and subatomic orbitals of the **AB1**. The frontier orbitals of both compounds are illustrated in Figure 4. The molecular orbital density of the HOMO and LUMO is especially arised from delocalized π -orbital of rings. The contribution to the HOMO and LUMO from nitro groups is significant that it results push-pull effect shown mostly in D- π -A molecules in the molecule **AB2** [68–70]. In the push-pull molecules, as a result of the withdrawing of the charge from the donor by the acceptor side of the molecule, the polarization is generated which provides the interaction between the donor and acceptor groups called intramolecular charge transfer (ICT). ICT process creates low energy molecular orbital as seen in the molecule **AB2**. Compared with **AB1**, conjugation of π orbitals is destroyed through incorporation of the nitrogroups to the molecules which cause a increase in the HOMO-LUMO energy gap. The HOMO- LUMO gaps for **AB1** and **AB2** are -4.87 eV and -3.73 eV, respectively.



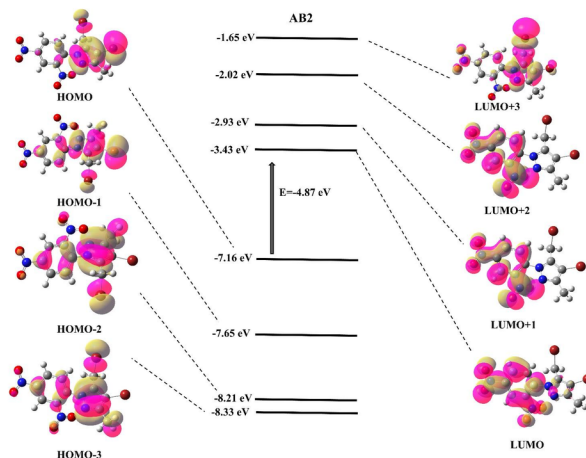


Figure 4. Selected frontier orbitals distributions of the both compounds.

Nitro groups affected the HOMO, LUMO, HOMO+1, HOMO+2, HOMO+3, LUMO-1, LUMO-2 and LUMO-3 molecular orbitals because of the discrepancy between molecular and crystal structures of the studied molecules. HOMO and HOMO-1 orbital of **AB1** were delocalized over the donor and acceptor moieties of the molecule while they were distributed over the pyrazole rings of the **AB2** as the electron-donating character of substituents increases. For the **AB1**, LUMO and LUMO+1 orbitals were localized over the donor and acceptor sides of the molecule whereas LUMO and LUMO+1 orbitals of the **AB2** mainly located electron acceptor groups. **AB2** displayed a major charge-transfer transition from a pyrazole ring delocalized HOMO and HOMO-1 to nitrophenyl ring delocalized LUMO and LUMO+1, due to efficient HOMO/LUMO overlap and the strong electron-withdrawing ability of the nitro groups.

UV-visible absorption spectra

The UV-visible absorption spectra of **AB1** and **AB2** are plotted in Figure 5 and the calculated maximum peak of the UV-visible absorption (λ_{abs}), excitation energy (E), oscillation strength (f), of the compounds **AB1** and **AB2** are summarized in Table 6. The peaks of the absorption spectra of the **AB2** ($\lambda_{\text{abs}} = 312$ nm) is red-shifted compared with the molecule **AB1** ($\lambda_{\text{abs}} = 287$ nm). It can be said that the introduced NO_2 groups has greatly affected the absorption spectra due to the increased intermolecular interactions in solid phase. The electronic excitations of both compounds are controlled by the transition from HOMO to LUMO.

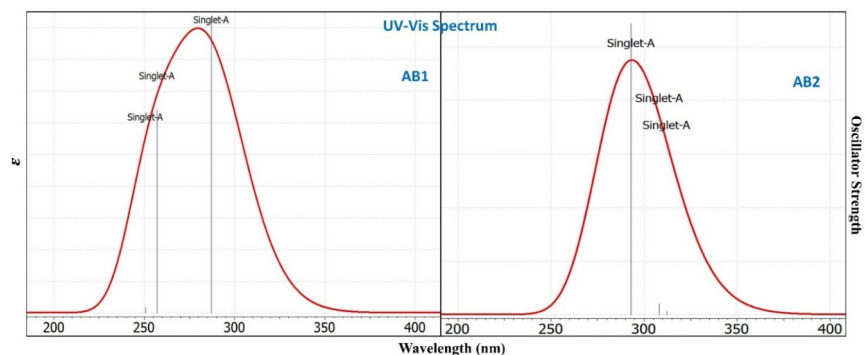


Figure 5. The calculated UV-vis Spektra of the molecule **AB1** and **AB2**.

Table 6. The calculated main peak of UV-vis absorption spectrum (λ_{abs}), excitation energy (E), oscillation strength (f), and major contributions.

Molecule	$\lambda_{\text{abs}}(\text{nm})$	$\Delta E(\text{eV})$	f	Major Contribution
AB1	287 257 250	-4.87 -4.82 -4.94	0.1864 0.1281 0.0036	H→L H-5 →L; H-4 →L+1 H-1 →L; H→L+1 H-2 →L+2; H-2 →L+1 H-1 →L+2; H→L+1 H→L+2
AB2	400 353 349	-3.0982 3.5056 3.5454	0.0359 0.0018 0.0402	H→L; H→L+1 H→L; H→L+1 H+1 →L; H-1 →L+1

Hirshfeld Surface Analysis

Hirshfeld surface analysis is the method to interpret the intermolecular interactions of the crystal structure by considering a fingerprint plot and a surface around the molecule [71–74]. A dnorm surface consisting of red-white-blue color provides comparison of intermolecular contacts relative to van der Waals radii. The hirshfeld surfaces and fingerprint plots of both compounds are shown in Figure 6 and Figure 7, respectively.

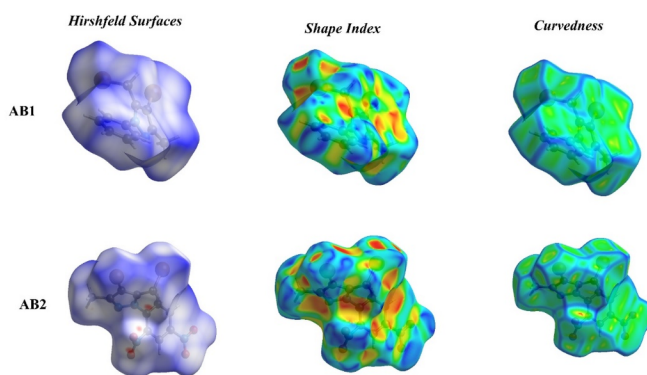


Figure 6. Views of the Hirshfeld surfaces for compounds, hirshfeld surfaces mapped with *shape-index* and curvedness for compounds.

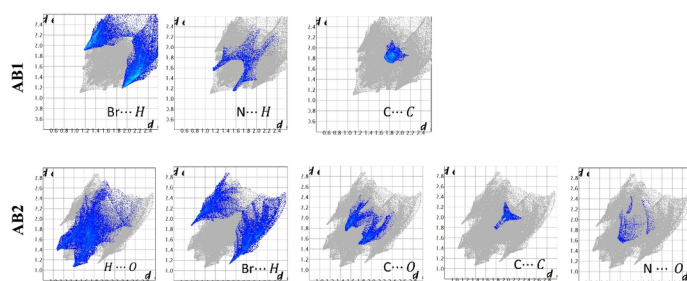


Figure 7. Fingerprint plots for compounds **AB1** and **AB2** .

Hirshfeld surface analysis shows that the $Br \cdots H$ contacts of the **AB2** is smaller than that of **AB1** ranging from 22.2% to 35.1% which represents short intermolecular short interactions between the neighboring molecules. For both molecules the $Br \cdots H$ and $H \cdots Br$ interactions are represented by a spike in the bottom left (donor) and right area of the fingerprint plot. The **AB2** displays a higher proportion of $O \cdots H$ (13.8%) than $H \cdots O$ (13.0%) interactions, and this is due to two of its phenyl protons interacting with the Br atoms. These brom-based interactions represent the closest contacts in the structure and can be viewed as a pair of large red spots on the dnorm surface. The deep red visible on the Hirshfeld surfaces are indicative of intermolecular $\pi \cdots \pi$ ($C \cdots C$) interactions, comprises 5.6% and 2.3% of the total Hirshfeld surfaces of **AB1** and **AB2**, respectively. Other visible bright red spots the total Hirshfeld surfaces of **AB2**, are due to intermolecular $O \cdots H$ contacts (comprised of 27.6%). The strong $O \cdots H$ contacts of the **AB2** is indicated by two adjacent deep-red region in the d_{norm} map. The $\pi \cdots \pi$ interactions about $Cg \cdots Cg$ which is the $C \cdots C$ contacts in the dnorm map are represented by another red spot . Due to the presence of adjacent red and blue triangles on the shape index surface, it can be said that $\pi \cdots \pi$ stacking interactions of the **AB1** and **AB2** are nearly

the same in their crystal structures. There is a flat region toward the bottom of both sides of the molecules which confirm the presence of the $\pi \cdots \pi$ stacking interactions. Convex region represented by blue triangles is due to the ring carbon atoms of the molecules and concave regions represented by red triangles is due to carbon atoms of the π stacked molecules.

Conclusion

In this work, we investigated the crystal structure, electronic structure and charge transport properties of two pyrazole derivatives through density functional theory and interpreted via Marcus Electron Theory. The optimized geometry structures, reorganization energy, absorption spectra, frontier orbitals, ionization potential (IP) and electronic affinity (EA) of both compounds were calculated to perform the relationship between the structure and property taking their crystal geometry, noncovalent interactions and aggregation modes in solid phase into account. According to SCXRD results the molecule **AB1** and **AB2** aggregate J type and antiparallel H type stacking modes in their solid phases which are favourable stacking modes to obtain high charge transfer rate due to high transfer integral. The incorporation of the NO_2 group to the molecule skeleton result in different crystal structure and packing arrangement therefore different charge transport property in terms of their reorganization energy. The hole reorganization energies of the both molecules are smaller than that of electron indicating that they can be used as *p*-type semiconductors. Since **AB2** exhibits lower hole reorganization energy than that of **AB1**, the charge transfer rate can be predicted high for **AB2**. In terms of its crystallographic data, it aggregates in strong antiparallel H type $\pi \cdots \pi$ stacking type with the small perpendicular distance between the adjacent rings. Therefore, this result consolidated that the molecule **AB2** can have high charge transport rate when it is used as an optoelectronic device. In addition, low-lying HOMOs, and high IPs of the **AB2** indicate the its better redox stability than **AB1**. Although this is case, beside the **AB2**, **AB1** shows preferred stacking mode in solid phase and low reorganization energy which is beneficial for device application. Accordingly, both molecules are suggested to be quite suitable for *p* type semiconducting materials with small reorganization energy and preferred stacking modes in solid phase.

Acknowledgement

This work was completed at Akdeniz University and Dokuz Eylül University. The author acknowledges Scientific Research Projects Coordination Unit of Akdeniz University (Project Number FDK-2016-1541), Dokuz Eylül University for the use of the Agilent Xcalibur Eos diffractometer (purchased under University Research Grant No: 2010.KB.FEN.13) and Assoc. Prof. Muhittin Aygün for his technical support in theoretical calculations.

Corresponding author

Gül Yakalı, gul.yakali@ikcu.edu.tr

Author contributions

Günseli Turgut Cin and Abdullah Biçer did synthesis and spectroscopic experiments of the both molecules and wrote synthesis part of the experimental section in the manuscript. Theoretical and single crystal x-ray diffraction studies were performed and written in the manuscript by Gül Yakalı. All authors reviewed the manuscript

Declarations

Conflict of interest

The authors declare that they have no conflict of interest.

Funding

The authors received no specific funding for this work.

References

1. Murphy AR, Fréchet JMJ (2007) Organic semiconducting oligomers for use in thin film transistors. *Chemical Reviews* 107:1066–1096. <https://doi.org/10.1021/cr0501386>
2. Kuo CH, Huang DC, Peng WT, et al (2014) Substituent effect on the crystal packing and electronic coupling of tetrabenzocoronenes: A structure-property correlation. *Journal of Materials Chemistry C* 2:3928–3935. <https://doi.org/10.1039/c4tc00296b>
3. Gelinck G, Heremans P, Nomoto K, Anthopoulos TD (2010) Organic transistors in optical displays and microelectronic applications. *Advanced Materials* 22:3778–3798. <https://doi.org/10.1002/adma.200903559>
4. Muccini M, Nazionale C (2006) PROGRESS ARTICLE A bright future for organic field-effect transistors. *Group* 605–613
5. Li Y, Guo Q, Li Z, et al (2010) Solution processable D - A small molecules for bulk-heterojunction solar cells. *Energy and Environmental Science* 3:1427–1436. <https://doi.org/10.1039/c003946b>
6. Jean R (2009) Molecular bulk heterojunctions: An emerging approach to organic solar cells. *Accounts of Chemical Research* 42:1719–1730. <https://doi.org/10.1021/ar900041b>
7. Liu J, Walker B, Tamayo A, et al (2013) Effects of heteroatom substitutions on the crystal structure, film formation, and optoelectronic properties of diketopyrrolopyrrole-based materials. *Advanced Functional Materials* 23:47–56. <https://doi.org/10.1002/adfm.201201599>
8. Carmen Ruiz Delgado M, Kim EG, Da Silva Filho DA, Bredas JL (2010) Tuning the charge-transport parameters of perylene diimide single crystals via end and/or core functionalization: A density functional theory investigation. *Journal of the American Chemical Society* 132:3375–3387. <https://doi.org/10.1021/ja908173x>
9. Zhang J, Ma Z, Zhang Q, et al (2013) Substitution effects on the electrical transporting properties of tetrathia[22]annulene[2,1,2,1]: Experimental and theoretical investigations. *Journal of Materials Chemistry C* 1:5765–5771. <https://doi.org/10.1039/c3tc30776j>
10. Zhang NX, Ren AM, Ji LF, et al (2018) Theoretical Investigations on Molecular Packing Motifs and Charge Transport Properties of a Family of Trialkylsilylethynyl-Modified Pentacenes/Anthradithiophenes. *Journal of Physical Chemistry C* 122:18880–18894. <https://doi.org/10.1021/acs.jpcc.8b06527>
11. Yang X, Wang L, Wang C, et al (2008) Influences of crystal structures and molecular sizes on the charge mobility of organic semiconductors: Oligothiophenes. *Chemistry of Materials* 20:3205–3211. <https://doi.org/10.1021/cm8002172>
12. Yao ZF, Wang JY, Pei J (2018) Control of π - π Stacking via Crystal Engineering in Organic Conjugated Small Molecule Crystals. *Crystal Growth and Design* 18:7–15. <https://doi.org/10.1021/acs.cgd.7b01385>
13. Shi YR, Wei HL, Jia XB, Liu YF (2018) Effects of crystal structures and intermolecular interactions on charge transport properties of organic semiconductors. *Journal of Materials Science* 53:15569–15587. <https://doi.org/10.1007/s10853-018-2719-0>
14. Wang K, Xie Y, Liu M, et al (2020) High-Contrast Polymorphic Luminogen Formed through Effect of Tiny Differences in Intermolecular Interactions on the Intramolecular Charge Transfer Process. *Advanced Optical Materials* 8:1–10. <https://doi.org/10.1002/adom.202000436>
15. Banerjee A, Saha A, Saha BK (2019) Understanding the Behavior of π - π Interactions in Crystal Structures in Light of Geometry Corrected Statistical Analysis: Similarities and Differences with the Theoretical Models. *Crystal Growth and Design* 19:2245–2252. <https://doi.org/10.1021/acs.cgd.8b01857>
16. Thomas R, Varghese S, Kulkarni GU (2009) The influence of crystal packing on the solid state fluorescence behavior of alkyloxy substituted phenyleneethynyls. *Journal of Materials Chemistry* 19:4401–4406. <https://doi.org/10.1039/b902937k>

17. Hermann J, Alfè D, Tkatchenko A (2017) Nanoscale π - π Stacked molecules are bound by collective charge fluctuations. *Nature Communications* 8:. <https://doi.org/10.1038/ncomms14052>
18. Li Q, Li Z (2020) Molecular Packing: Another Key Point for the Performance of Organic and Polymeric Optoelectronic Materials. *Accounts of Chemical Research* 53:962–973. <https://doi.org/10.1021/acs.accounts.0c00060>
19. Yang J, Ren Z, Chen B, et al (2017) Three polymorphs of one luminogen: How the molecular packing affects the RTP and AIE properties? *Journal of Materials Chemistry C* 5:9242–9246. <https://doi.org/10.1039/c7tc03656f>
20. Huang R, Liu H, Liu K, et al (2019) Marriage of Aggregation-Induced Emission and Intramolecular Charge Transfer toward High Performance Film-Based Sensing of Phenolic Compounds in the Air. *Analytical Chemistry*. <https://doi.org/10.1021/acs.analchem.9b03096>
21. Sutton C, Risko C, Brédas JL (2016) Noncovalent Intermolecular Interactions in Organic Electronic Materials: Implications for the Molecular Packing vs Electronic Properties of Acenes. *Chemistry of Materials* 28:3–16. <https://doi.org/10.1021/acs.chemmater.5b03266>
22. Wang K, Zhang H, Chen S, et al (2014) Organic polymorphs: One-compound-based crystals with molecular-conformation- and packing-dependent luminescent properties. *Advanced Materials* 26:6168–6173. <https://doi.org/10.1002/adma.201401114>
23. Li J, Wang M, Ren S, et al (2012) High performance organic thin film transistor based on pentacene derivative: 6,13-dichloropentacene. *Journal of Materials Chemistry* 22:10496–10500. <https://doi.org/10.1039/c2jm16871e>
24. Yoon S, Chung JW, Gierschner J, et al (2010) [mechano][AIEE]Park-DBDCS(JACS-2010).pdf. 13675–13683. <https://doi.org/10.1021/ic902591s.9>
25. Fraboni B, Fraleoni-Morgera A, Geerts Y, et al (2016) Organic single crystals: An essential step to new physics and higher performances of optoelectronic devices. *Advanced Functional Materials* 26:2229–2232. <https://doi.org/10.1002/adfm.201504924>
26. Varghese S, Das S (2011) Role of molecular packing in determining solid-state optical properties of π -conjugated materials. *Journal of Physical Chemistry Letters* 2:863–873. <https://doi.org/10.1021/jz200099p>
27. Xie Z, Yang B, Li F, et al (2005) Cross dipole stacking in the crystal of distyrylbenzene derivative: The approach toward high solid-state luminescence efficiency. *Journal of the American Chemical Society* 127:14152–14153. <https://doi.org/10.1021/ja054661d>
28. 30.pdf
29. Hunter CA (1993) Arene—Arene Interactions: Electrostatic or Charge Transfer? *Angewandte Chemie International Edition in English* 32:1584–1586. <https://doi.org/10.1002/anie.199315841>
30. Hunter CA MELDOLA LECTURE. The Role
31. Kumar NSS, Gujrati MD, Wilson JN (2010) Evidence of preferential π -stacking: A study of intermolecular and intramolecular charge transfer complexes. *Chemical Communications* 46:5464–5466. <https://doi.org/10.1039/c0cc00249f>
32. Cariati E, Lanzeni V, Tordin E, et al (2011) Efficient crystallization induced emissive materials based on a simple push-pull molecular structure. *Physical Chemistry Chemical Physics* 13:18005–18014. <https://doi.org/10.1039/c1cp22267h>
33. Zhang H, Zhang Z, Ye K, et al (2006) Organic crystals with tunable emission colors based on a single organic molecule and different molecular packing structures. *Advanced Materials* 18:2369–2372. <https://doi.org/10.1002/adma.200600704>

34. Li NZ, Li C, Coordination S (2020) Crystallization Induced Enhanced Emission in Two
35. Cias P, Slugovc C, Gescheidt G (2011) Hole transport in triphenylamine based OLED devices: From theoretical modeling to properties prediction. *Journal of Physical Chemistry A* 115:14519–14525. <https://doi.org/10.1021/jp207585j>
36. Jia X, Wei H, Shi Y, Liu Y (2019) Theoretical studies on charge transport and optical properties of diarylmalesic anhydride derivatives as organic light-emitting materials. *Chemical Physics Letters* 724:50–56. <https://doi.org/10.1016/j.cplett.2019.03.053>
37. Wang L, Duan G, Ji Y, Zhang H (2012) Electronic and charge transport properties of perixanthoxanthene: The effects of heteroatoms and phenyl substitutions. *Journal of Physical Chemistry C* 116:22679–22686. <https://doi.org/10.1021/jp306326e>
38. Siddiqui SA, Al-Hajry A, Al-Assiri MS (2016) Ab initio investigation of 2,2'-bis(4-trifluoromethylphenyl)-5,5'-bithiazole for the design of efficient organic field-effect transistors. *International Journal of Quantum Chemistry* 116:339–345. <https://doi.org/10.1002/qua.25034>
39. Zhang M, Zhao G (2012) Ming-Xing Zhang and Guang-Jiu Zhao *
40. Wang L, Li T, Shen Y, Song Y (2016) A theoretical study of the electronic structure and charge transport properties of thieno[2,3-b]benzothiophene based derivatives. *Physical Chemistry Chemical Physics* 18:8401–8411. <https://doi.org/10.1039/c5cp07879b>
41. Tripathi A, Prabhakar C (2019) Optoelectronic and charge-transport properties of truxene, isotruxene, and its heteroatomic (N, O, Si, and S) analogs: A DFT study. *Journal of Physical Organic Chemistry* 32:88–96. <https://doi.org/10.1002/poc.3944>
42. Qi Y, Chen C, Zheng C, et al (2020) Heteroatom-bridged heterofluorenes: A theoretical study on molecular structures and optoelectronic properties. *Physical Chemistry Chemical Physics* 22:3675–3682. <https://doi.org/10.1039/c9cp06458c>
43. Yan L, Zhao Y, Yu H, et al (2016) Influence of heteroatoms on the charge mobility of anthracene derivatives. *Journal of Materials Chemistry C* 4:3517–3522. <https://doi.org/10.1039/c6tc01088a>
44. Chai S, Wen SH, Huang JD, Han KL (2011) Density functional theory study on electron and hole transport properties of organic pentacene derivatives with electron-withdrawing substituent. *Journal of Computational Chemistry* 32:3218–3225. <https://doi.org/10.1002/jcc.21904>
45. Bonacorso HG, Dal Forno GM, Wiethan C, et al (2017) Sequential one-pot three-step synthesis of poly-substituted 4-(5-(trifluoromethyl)-1H-pyrazol-4-yl)-1H-1,2,3-triazole systems. *RSC Advances* 7:43957–43964. <https://doi.org/10.1039/c7ra07960e>
46. Ma HJ, Li YH, Zhao QF, et al (2010) Synthesis and herbicidal activity of novel N-(2,2,2)-trifluoroethylpyrazole derivatives. *Journal of Agricultural and Food Chemistry* 58:4356–4360. <https://doi.org/10.1021/jf9042166>
47. Li Y, Liu Y, Xu G, et al (2014) A combined experimental and natural bonding orbital charges study on the one-pot regioselective synthesis of 4-chloropyrazoles. *Journal of Chemical Research* 38:658–661. <https://doi.org/10.3184/174751914X14137288281925>
48. Yamamoto S, Tomita N, Suzuki Y, et al (2012) Design, synthesis, and biological evaluation of 4-arylmethyl-1-phenylpyrazole and 4-aryloxy-1-phenylpyrazole derivatives as novel androgen receptor antagonists. *Bioorganic and Medicinal Chemistry* 20:2338–2352. <https://doi.org/10.1016/j.bmc.2012.02.005>
49. Baker D (2013) CrysAlis Pro responsible. 44:
50. Sheldrick GM (2015) Crystal structure refinement with SHELXL. *Acta Crystallographica Section C: Structural Chemistry* 71:3–8. <https://doi.org/10.1107/S2053229614024218>

51. Sheldrick GM (2015) SHELXT - Integrated space-group and crystal-structure determination. *Acta Crystallographica Section A: Foundations of Crystallography* 71:3–8. <https://doi.org/10.1107/S2053273314026370>
52. Dolomanov O V., Bourhis LJ, Gildea RJ, et al (2009) OLEX2: A complete structure solution, refinement and analysis program. *Journal of Applied Crystallography* 42:339–341. <https://doi.org/10.1107/S0021889808042726>
53. Superzeure EX, Superieure EX (1964) *J. Chem. Phys.* 155:
54. Tsiper E V., Soos ZG, Gao W, Kahn A (2002) Electronic polarization at surfaces and thin films of organic molecular crystals: PTCDA. *Chemical Physics Letters* 360:47–52. [https://doi.org/10.1016/S0009-2614\(02\)00774-1](https://doi.org/10.1016/S0009-2614(02)00774-1)
55. Taydakov I V., Akkuzina AA, Avetisov RI, et al (2016) Effective electroluminescent materials for OLED applications based on lanthanide 1,3-diketones bearing pyrazole moiety. *Journal of Luminescence* 177:31–39. <https://doi.org/10.1016/j.jlumin.2016.04.017>
56. Irfan A, Al-Sehemi AG, Chaudhry AR, et al (2016) The structural, electro-optical, charge transport and nonlinear optical properties of 2-[(3,5-dimethyl-1-phenyl-1H-pyrazol-4-yl)methylidene]indan-1,3-dione. *Optik* 127:10148–10157. <https://doi.org/10.1016/j.ijleo.2016.08.007>
57. Moia D, Vaissier V, López-Duarte I, et al (2014) The reorganization energy of intermolecular hole hopping between dyes anchored to surfaces. *Chemical Science* 5:281–290. <https://doi.org/10.1039/c3sc52359d>
58. Li H, Duan L, Zhang D, Qiu Y (2014) Influence of molecular packing on intramolecular reorganization energy: A case study of small molecules. *Journal of Physical Chemistry C* 118:14848–14852. <https://doi.org/10.1021/jp504979x>
59. Chang Y, Chao I (2010) An Important Key to Design Molecules with Small Internal Reorganization Energy: Strong Nonbonding Character in Frontier Orbitals. 116–121. <https://doi.org/10.1021/jz900042x>
60. Gao H (2010) Theoretical investigation into charge mobility. 759–763. <https://doi.org/10.1007/s00214-010-0804-9>
61. Qiu M, Pei W, Lu Q, et al (2019) DFT characteristics of charge transport in DBTP-based hole transport materials. *Applied Sciences (Switzerland)* 9:1–7. <https://doi.org/10.3390/app9112244>
62. Brückner C, Walter C, Stolte M, et al (2017) Structure – Property Relationships for Exciton and Charge Reorganization Energies of Dipolar Organic Semiconductors : A Combined Valence Bond Self-Consistent Field and Time-Dependent Hartree-Fock and DFT Study of Merocyanine Dyes To cite this version : HA
63. Lin BC, Cheng CP, Lao ZPM (2003) Reorganization energies in the transports of holes and electrons in organic amines in organic electroluminescence studied by density functional theory. *Journal of Physical Chemistry A* 107:5241–5251. <https://doi.org/10.1021/jp0304529>
64. Wang C, Dong H, Hu W, et al (2012) Semiconducting π -conjugated systems in field-effect transistors: A material odyssey of organic electronics. *Chemical Reviews* 112:2208–2267. <https://doi.org/10.1021/cr100380z>
65. Zheng Z, Yu Z, Yang M, et al (2013) Substituent group variations directing the molecular packing, electronic structure, and aggregation-induced emission property of isophorone derivatives. *Journal of Organic Chemistry* 78:3222–3234. <https://doi.org/10.1021/jo400116j>
66. Ji LF, Fan JX, Zhang SF, Ren AM (2017) Theoretical investigations into the charge transfer properties of thiophene α -substituted naphthodithiophene diimides: Excellent n-channel and ambipolar organic semiconductors. *Physical Chemistry Chemical Physics* 19:13978–13993. <https://doi.org/10.1039/c7cp01114h>

67. Hutchison GR, Ratner MA, Marks TJ (2005) Intermolecular charge transfer between heterocyclic oligomers. Effects of heteroatom and molecular packing on hopping transport in organic semiconductors. *Journal of the American Chemical Society* 127:16866–16881. <https://doi.org/10.1021/ja0533996>
68. Wang H, Liu H, Bai FQ, et al (2015) Theoretical and experimental study on intramolecular charge-transfer in symmetric bi-1,3,4-oxadiazole derivatives. *Journal of Photochemistry and Photobiology A: Chemistry* 312:20–27. <https://doi.org/10.1016/j.jphotochem.2015.07.006>
69. Parusel ABJ (2001) Excited state intramolecular charge transfer in N,N -heterocyclic-4-aminobenzonitriles: A DFT study. *Chemical Physics Letters* 340:531–537. [https://doi.org/10.1016/S0009-2614\(01\)00441-9](https://doi.org/10.1016/S0009-2614(01)00441-9)
70. Shee J, Head-Gordon M (2020) Predicting Excitation Energies of Twisted Intramolecular Charge-Transfer States with the Time-Dependent Density Functional Theory: Comparison with Experimental Measurements in the Gas Phase and Solvents Ranging from Hexanes to Acetonitrile. *Journal of Chemical Theory and Computation* 16:6244–6255. <https://doi.org/10.1021/acs.jctc.0c00635>
71. Saeed A, Bolte M, Erben MF, Pérez H (2015) Intermolecular interactions in crystalline 1-(adamantane-1-carbonyl)-3-substituted thioureas with Hirshfeld surface analysis. *CrystEngComm* 17:7551–7563. <https://doi.org/10.1039/c5ce01373a>
72. Seth SK, Sarkar D, Jana AD, Kar T (2011) On the possibility of tuning molecular edges to direct supramolecular self-assembly in coumarin derivatives through cooperative weak forces: Crystallographic and hirshfeld surface analyses. *Crystal Growth and Design* 11:4837–4849. <https://doi.org/10.1021/cg2006343>
73. Seth SK (2014) Structural elucidation and contribution of intermolecular interactions in O-hydroxy acyl aromatics: Insights from X-ray and Hirshfeld surface analysis. *Journal of Molecular Structure* 1064:70–75. <https://doi.org/10.1016/j.molstruc.2014.01.068>
74. Seth SK, Sarkar D, Roy A, Kar T (2011) Insight into supramolecular self-assembly directed by weak interactions in acetophenone derivatives: Crystal structures and Hirshfeld surface analyses. *CrystEngComm* 13:6728–6741. <https://doi.org/10.1039/c1ce05670k>